Finite Element Analysis of a Deformable Array Transducer

Loriann L. Ries and Stephen W. Smith, *Member, IEEE*

Abstract—**Deformable array transducers have previously been described to implement 2-D phase aberration correction of near-field aberrators with only a 1 × N or 2 × N array configuration. This transducer design combines mechanical phase correction using an actuator with electronic phase correction for a 2-D correction with significantly fewer elements than a full 2-D array. We have previously reported the fabrication and results of a 1 × 32 deformable array fabricated with a RAINBOW (Reduced And INternally Biased Wafer) actuator. Because of the complicated construction of deformable arrays, we propose to use finite element analysis (FEA) as a design tool for array development. In this paper, we use 2-D and 3-D FEA to model the experimental results of the deformable array as the first step toward development of a design tool.**

Because the deformable array combines a mechanical actuator with a medical ultrasound transducer, improvement in performance must consider both the ultrasound characterization along with the low frequency actuator characterization. For the ultrasound characterization, time domain FEA simulations of electrical vector impedance accurately predicted the measurements of single array elements. Additionally, simulations of pulse-echo sensitivity and bandwidth were also well matched to measurements.

For the low frequency actuator characterization, time domain simulation of the low frequency vector impedance accurately predicted measurement and confirmed the fundamental flexure resonance of the cantilever configuration at 1.3 kHz. Frequency domain FEA included thermal processing effects and predicted actuator curvature arising during fabrication. Finally, frequency domain FEA simulations of voltage-induced displacement accurately predicted measured displacement.

I. Introduction

Phase aberration correction is the process of compensating for acoustic velocity inhomogeneities in tissue to improve the spatial resolution of medical ultrasound images. Assuming the aberrating tissue is close to the face of the transducer, such as subcutaneous fat, near-field correction algorithms can then be applied to restore the image. These algorithms provide correction by adjusting the electronic phase delays used to steer and focus the ultrasound beam. Using an electronic correction technique, a 2-D correction would require a 2-D array. Instead of using a 2-D array for phase correction, we have described a deformable array transducer design using actuators to implement 2-D phase correction with a 1 × N or 2 × N array [1], [2].

Manuscript received July 31, 1997; accepted May 27, 1999. This work was supported in part by NIH grant CA-56475 and NSF grants CDR-8622201 and BES-15342.

L. L. Ries is with ATL Ultrasound, Bothell, WA 98021.

S. W. Smith is with Duke University, Durham, NC 27708.

The deformable transducer design is similar to a technique used in adaptive optics to restore the spatial resolution of astronomical telescopes [3]. Because of turbulence in the upper atmosphere, planar wavefronts of light from distant stars are disrupted in a manner similar to aberrating tissue in ultrasound. To restore the resolution of the telescope, the aberrating phase profile is measured and applied to mechanical actuators that warp a flexible mirror, compensating for the turbulence. For ultrasound, we have proposed a hybrid phase correction method that combines mechanical phase correction, similar to the telescope mirror, with electronic phase correction for a 2-D phase correction with a 1 × N array. An example of mechanical phase correction in elevation is shown in Fig. 1. The schematic drawing in Fig. 1(a) shows the elevation profile of a linear deformable array with aberrating tissue in front of the elements. Because of the large elevation dimension of the linear array, the effect of the aberrator is averaged in elevation. Therefore, these elements cannot be used to implement electronic phase correction in elevation. An example of a corrected position is shown in Fig. 1(b). The elements have been tilted in elevation using an actuator to compensate for the linear component of the aberrating tissue. By combining mechanical phase correction in elevation, tilting the elements using an actuator, with electronic phase correction in azimuth, a 2-D correction can be implemented with a 1 × N deformable array [1], [4].

We have previously reported the fabrication and results of a 1 × 32 deformable array constructed using a low frequency piezoelectric actuator called a RAINBOW (Reduced And INternally Biased Wafer) [2]. A RAINBOW is a piezoelectric ceramic that has been chemically reduced on one side to create a monolithic unimorph actuator [5]. Because the actuators are fabricated using PZT, they can be used to induce the physical element displacement along with transmitting and receiving the ultrasound pulses. B-scan images of a cyst in a tissue-mimicking phantom were made with the array, and phase correction was simulated by tilting the elements in elevation. Cyst contrast measurements increased from 0.76 when one-half of the elements were tilted 1° to a contrast of 0.86 for the phase-corrected case with all of the elements restored to the level position.

We have also proposed using the deformable array configuration to achieve an electronically adjustable transmit elevation focus or possibly receive mode dynamic elevation focusing. If the deformable array elements were curved with a focus useful for imaging, then the elevation focus could be altered by tilting the elements in elevation. The possibility of using the deformable array elements for ei-

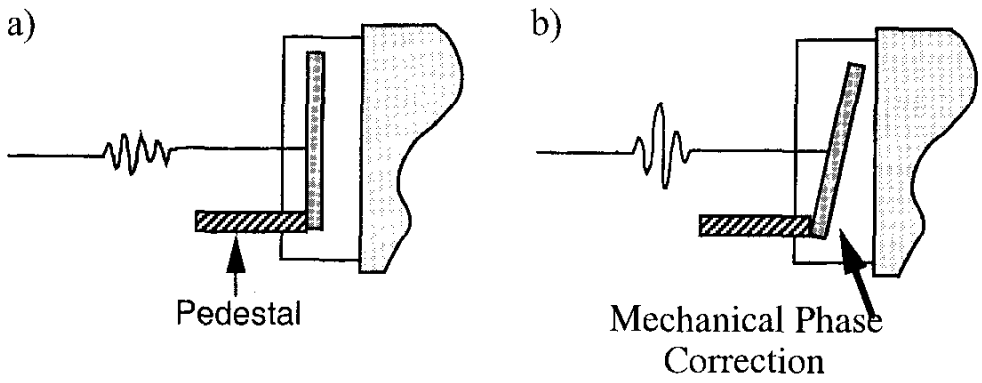

Fig. 1. Elevation profile of a $1 \times N$ deformable array without phase correction (a) or with the elements tilted for mechanical phase correction (b).

ther an adjustable or dynamic focus is dependent on the speed of the actuator response.

To improve the performance of the deformable array, both the low frequency actuator characteristics and the ultrasonic characteristics must be considered. Therefore, we would like to use finite element analysis (FEA) as a design tool for deformable array development. In this paper, we hypothesize that 2-D and 3-D FEA can be used to model the ultrasonic characteristics as well as the low frequency actuator characteristics of the 1×32 deformable array.

For the ultrasonic characterization, we have modeled elements of the array using the time domain code of PZFlex developed by Weidlinger Associates, Inc. (New York, NY and Los Altos, CA). We have compared the simulated vector impedance of free single elements and array elements with measured impedance. Additionally, we have compared the simulated pulse-echo response and corresponding power spectrum of an array element with measured values.

For the actuator characterization, we have used both PZFlex and ANSYS (Swanson Analysis Systems, Inc., Houston, PA) to model array elements. PZFlex was used to simulate the low frequency vector impedance of array elements and was compared with measured values to verify the flexure mode of the actuator. ANSYS was used to model the thermal properties of the RAINBOW ceramic during the cooling process of the actuator fabrication. The thermal stresses developed upon cooling influence the actuator deflection. Using ANSYS, we have modeled the voltage-induced displacement of the actuator and compared the simulated results with measured values.

II. Methods

A. Actuator Background

The RAINBOW actuators were developed by Haertling *et al.* [5] and have been analyzed by investigators at Clemson and Pennsylvania State University [6]–[8]. A RAINBOW is fabricated by heating a piezoelectric ceramic to approximately 975°C on a graphite block, resulting in a chemical reduction of a layer of the ceramic. The reduced layer is largely composed of lead and is no longer piezoelectric. The resulting actuator is similar to a unimorph [9] with an active piezoelectric layer and a mechanical support provided by the reduced layer.

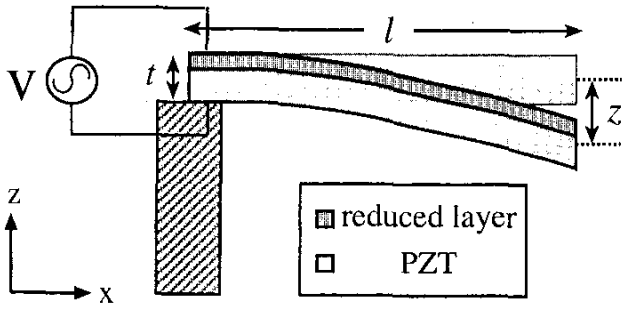

Fig. 2. Schematic diagram of the deflection of a RAINBOW unimorph actuator.

When a unimorph actuator, such as a RAINBOW, is mounted in a cantilever configuration, the free end of the actuator deflects in response to applied voltage as shown in Fig. 2. Following the development of Smits [10], [11], the theoretical free deflection of a unimorph can be derived. The strain in the piezoelectric layer , S_1^P, can be written from the constitutive equations for piezoelectricity as

$$S_1^P = s_{11}^P T_1 + d_{31} E_3 \tag{1}$$

where s_{11}^P is the compliance of the piezoelectric layer, T_1 is the stress, d_{31} is the piezoelectric constant, and E_3 is the electric field. Similarly, the strain in the reduced layer, S_1^R, can be written as

$$S_1^R = s_{11}^R T_1 \tag{2}$$

where s_{11}^R is the compliance of the reduced layer and T_1 is the stress. When voltage is applied across the piezoelectric layer, the PZT expands or contracts. Because the reduced layer is not piezoelectric, the movement of the piezoelectric layer is resisted along the interface of the two materials, which results in bending of the free tip of the actuator. At

equilibrium, the strain at the boundary between the PZT and reduced layer must be equal. Because of the applied voltage, there is a force, F, and a moment, M, acting on each layer. To denote the difference between the two layers, a superscript P specifies the piezoelectric layer, and a superscript R specifies the reduced layer. The equivalence of the strain at the boundary is then given by

$$\frac{F^P s_{11}^P}{w t_{\mathrm{PZT}}} + \frac{t_{\mathrm{PZT}} M^P}{2 Y^P I^P} + d_{31} E_3 = -\frac{F^R s_{11}^R}{w t_{\mathrm{redc}}} - \frac{t_{\mathrm{redc}} M^R}{2 Y^R I^R} \quad (3)$$

where w is the width of the actuator; t_{PZT} and t_{redc} are the thickness of the piezoelectric layer and reduced layer, respectively; Y is the Young's modulus; and I is the moment of inertia. Because there is no displacement in the x-direction at equilibrium, the force on the piezoelectric layer is equal to the force on the reduced layer. Therefore, the superscripts that distinguish the force may be dropped.

The moments acting on the reduced and piezoelectric layers can be related through the radius of curvature $1/R$. Because both layers are thin, the radius of curvature is assumed to be the same in both layers and can be written as

$$\frac{1}{R} = \frac{M^P}{Y^P I^P} = \frac{M^R}{Y^R I^R} \quad (4)$$

where Y is equal to $1/s_{11}$ and I is equal to $wt^3/12$.

At the free end of the actuator, the sum of all moments must be 0, and, therefore,

$$M^P + M^R = F\frac{(t_{\mathrm{PZT}} + t_{\mathrm{redc}})}{2}. \quad (5)$$

Using (4) and (5), the moments can be written as a function of the force F. Substituting the moments into (3), the force F can be written as shown in (6) (top of next page).

To solve for the free deflection of the actuator, the radius of curvature for the deflection of a beam can be written as (7) for small deflections:

$$\frac{1}{R} = \frac{d^2 z}{dx^2} = \frac{M^P}{Y^P I^P} \quad (7)$$

where z is the vertical displacement of the actuator and x is the length along the actuator. Integrating twice with respect to x will yield the free displacement of the actuator (z) as a function of the length (x). Substituting the total length of the actuator ($x = l$), the free tip displacement can be calculated. After rearranging and simplifying, the displacement can be written as

$$z = \frac{3}{2}\frac{l^2}{t_{\mathrm{PZT}}^2} k_d d_{31} V \quad (8)$$

where d_{31} is the piezoelectric coefficient of the ceramic, l is the length of the actuator, t_{PZT} is the thickness of the piezoelectric layer, k_d is the displacement coefficient accounting for the neutral axis of the unimorph, and V is the applied voltage. The displacement coefficient, k_d, is calculated using

$$k_d = \frac{2xy(1+x)}{1 + 4xy + 6x^2 y + 4x^3 y + x^4 y^2}; \quad x = \frac{t_{\mathrm{redc}}}{t_{\mathrm{PZT}}} \text{ and } y = Y_{\mathrm{redc}} s_{11}^E \quad (9)$$

where t_{redc} is the thickness of the reduced layer, t_{PZT} is the thickness of the piezoelectric layer, Y_{redc} is the Young's modulus of the reduced layer, and s_{11}^E is the mechanical compliance of the PZT [12]. For the RAINBOW used in this study, k_d was calculated to be 0.283 with a t_{redc} of 0.16 mm, t_{PZT} of 0.22 mm, Y_{redc} of 5.88×10 N/m^2, and s_{11}^E of 16.5×10^{-12} m^2/N.

The RAINBOW actuator differs from a conventional unimorph by the presence of internal stresses. Because of the different coefficients of thermal expansion of the reduced and piezoelectric layers, combined with the reduction in volume of the reduced layer, the actuator takes on a curved shape when cooled to room temperature. The internal stresses developed during the cooling process enhance the low frequency displacement characteristics of the actuator caused by stress-induced domain reorientation [13]. The stress-induced domain reorientation, or stress biasing, results in an effective d_{31}, which varies through the thickness of the actuator [14]. To account for the relative change in d_{31} and enhanced displacement because of stress biasing, (8) can be multiplied by k_p. The free deflection of a RAINBOW can then be predicted by [12]:

$$z = \frac{3}{2}\frac{l^2}{t_{\mathrm{PZT}}^2} k_d k_p d_{31} V. \quad (10)$$

Currently, the theoretical basis for k_p is still being investigated [14]. However, the value of k_p can be determined experimentally by measuring the free tip displacement of the actuator as a function of the applied voltage.

Another important actuator characteristic is the frequency of the fundamental flexure resonance of the cantilever configuration. For the deformable array, the fundamental flexure resonance will set the upper limit of the speed of elevation phase correction and elevation focusing. The flexure resonance of the RAINBOW can be predicted by (assuming $l \gg w$ and $\rho_{\mathrm{PZT}} = \rho_{\mathrm{redc}}$) [15]:

$$f = \frac{2\beta_0 t_{\mathrm{PZT}} N_1^E}{l^2}\sqrt{\frac{2xy}{k_d(1+xy)}} \quad (11)$$

where $\beta_0 = 0.16$ for cantilever mounting, N_1^E is the frequency constant of the PZT (1420 Hz-m for PZT 5H), w is the width of the element, and ρ is the density of the reduced or piezoelectric layer. Overtone frequencies of the fundamental resonance can be predicted by multiplying the fundamental frequency by 6.3, 18, or 34 for the first, second, and third overtones, respectively [16].

B. Transducer Description

The RAINBOW actuator used to build the 1×32 deformable array was manufactured by Aura Ceramics, Inc.

$$F = \frac{-d_{31}E_3 w t_{\mathrm{PZT}} t_{\mathrm{rede}} \left(t_{\mathrm{PZT}}^3 s_{11}^R + t_{\mathrm{rede}}^3 s_{11}^P\right)}{\left(t_{\mathrm{PZT}}^4 \left(s_{11}^R\right)^2 + 4t_{\mathrm{PZT}}^3 s_{11}^P s_{11}^R t_{\mathrm{rede}} + 6t_{\mathrm{PZT}}^2 s_{11}^P s_{11}^R t_{\mathrm{rede}}^2 + 4t_{\mathrm{PZT}} s_{11}^P s_{11}^R t_{\mathrm{rede}}^3 + t_{\mathrm{rede}}^4 \left(s_{11}^P\right)^2\right)}. \quad (6)$$

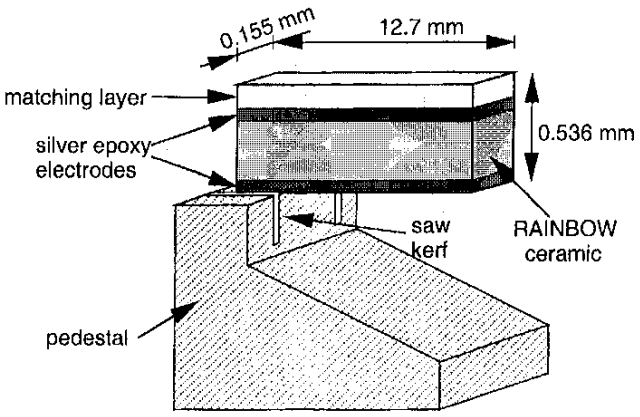

Fig. 3. Diagram of a single element of the 1 × 32 deformable array.

(New Hope, MN) using C3900 PZT. Their C3900 formulation is analogous to PZT 5H. For the deformable array, the RAINBOW was used to generate and receive ultrasound pulses along with creating the physical element displacement. A diagram of a single element of the array can be found in Fig. 3. We have previously described the array fabrication [2].

The element was mounted in a cantilever configuration with a light epoxy pedestal constraining approximately 2 mm of the 12.7-mm long element. The RAINBOW actuator was 0.38 mm thick with 0.04-mm electrodes of silver epoxy. A 0.076-mm thick quarter wavelength matching layer of Ablefilm conductive epoxy (Ablestick, Rancho Dominguez, CA) was bonded to the top of the element.

C. Transducer Measurements

The ultrasonic characterization of the deformable array included measurements of vector impedance, pulse-echo sensitivity, and pulse-echo spectrum. The element resonances were determined with measurements of vector impedance in air with a vector impedance meter. For the sensitivity measurements, the elements were driven with a 100-Vpp, 4.2-MHz, two-cycle sine wave from a signal source with an rf power amplifier. The return echo was reflected from a flat aluminum block, 5 cm from the transducer face, and was received from an adjacent element with a scope probe (10 Mohms; 11 pF). The corresponding power spectrum was measured using a stepless gate and a spectrum analyzer.

The actuator characterization included measurements of low frequency vector impedance, initial curvature, and voltage-induced displacement. The fundamental flexure resonance and overtone frequencies were determined by measuring the low frequency (1 to 30 kHz) vector impedance of single elements in air with a vector impedance meter. To determine the initial curvature of the RAINBOW elements, the displacement of the free tip of the actuator was measured with a thickness gauge. Finally, the voltage induced displacement was measured by applying a DC voltage to the actuator elements using a high voltage power supply and measuring the displacement of the free tip of the element with a calibrated microscope micrometer.

D. Finite Element Modeling

Our FEA of the RAINBOW elements can be separated into two areas: the ultrasonic analysis and the low frequency actuator analysis. Many researchers have successfully used FEA to model both ultrasound transducers [17]–[21] and actuators [14], [22–24].

1. Ultrasound Characterization: For the ultrasonic analysis, we chose to use the explicit time-domain code PZFlex. PZFlex has already been shown to model linear array elements and multilayer 1.5-D array elements accurately [20], [25].

The ultrasonic analysis included simulations of vector impedance, resonance mode shapes, and pulse-echo response. To calculate the impedance, the model was driven with an approximated impulse of a one-half cycle sine wave at 7.5 MHz to provide a broadband excitation spectrum encompassing the frequency range of interest. For each time step, the voltage, $V(t)$, and the charge, $Q(t)$, were computed at the electrodes of the model, and the model was executed until the voltage and charge decayed to 0. The charge, $Q(t)$, was then numerically differentiated to calculate the current $I(t)$. The impedance was calculated from

$$Z(f) = \frac{F\{V(t)\}}{F\{I(t)\}} \quad (12)$$

where $Z(f)$ is the complex impedance and $F\{\}$ represents the Fourier transform. The minima and maxima of the impedance are identified as the resonance and antiresonance frequencies, respectively.

It is typically of interest to determine the resonance shapes associated with the identified resonance frequencies as described previously. The time domain analysis can be re-executed with the additional output of the resonance shapes calculated at the previously determined resonance frequencies. The resonance shapes are calculated by a discrete Fourier transform of the nodal velocities and can be animated to show the modal oscillation or displayed as two pictures of displacement extrema that are 180 degrees out of phase. This approach to the calculation of resonance shapes is well suited within the overall explicit

time-domain scheme used by PZFlex [26]. The results obtained are analogous to those obtained from a classic eigenproblem formulation. With a conservative system, the results correspond to an eigenproblem with real eigenmodes. When material or radiation damping exists in the model, the equivalence is extended to an eigenproblem with complex eigenmodes.

The simulation of the pulse-echo response off a flat reflecting plate in water was also completed. This feature, available in PZFlex [26] and first described by Lerch *et al.* [27], is based on the Kirchoff integral equation. To calculate the response, the problem is separated into a transmit calculation and a receive calculation. The transmit portion calculated the pressure and its normal gradient at a plane located in the water, close to the face of the transducer. Using Kirchhoff extrapolation, the echo return signal caused by a flat, infinite, rigid reflector at a specified distance from the transducer is calculated. The receive portion then uses the calculated echo as an applied boundary condition, or incident wave, on the top surface of the model, or the water layer. Reflections from all interfaces are thus inherent in the calculation. In addition, electrical circuits may also be modeled on both transmit and receive calculations. The response of the model to the echo impinging on the top surface of the transducer is the pulse-echo response. The power spectrum of the pulse can then be calculated from

$$P(f) = |F\{\text{pulse}(t)\}|^2 \tag{13}$$

where $P(f)$ is the power spectrum and $F\{\}$ represents the Fourier transform.

2. Low Frequency Actuator Characterization: For the actuator analysis, PZFlex was used to calculate the low frequency complex impedance to verify the resonant frequencies of the flexure mode of the actuator. However, the initial curvature of the actuator, which produces the internal stresses, and low frequency displacement must also be modeled. To model both the initial curvature and displacement of the actuator, the thermal properties of the RAINBOW during cool down must be included. Currently, static thermal processing is not available in PZFlex. Therefore, we chose to use ANSYS for the displacement analysis. Using ANSYS, we calculated the displacement of the actuator model caused by thermal processing and applied voltage.

E. Material Properties

The FEA of the RAINBOW elements required several different materials to be modeled. The piezoelectric layer was modeled using the material properties of PZT 5H, whereas the reduced layer, silver epoxy electrodes, conductive matching layer, and epoxy stand were modeled as elastic materials. A summary of the material properties used in the ultrasonic analysis is given in the Appendix.

For the low frequency actuator analysis, d_{31} must be modified to account for the internal stress biasing caused by thermal processing. To do this, k_p was calculated by applying (10) to the measurements of free tip displacement of the actuator versus voltage. From our experimental results, k_p was determined to be 2.7. To account for k_p in the simulations, the normal piezoelectric coefficient, $d_{31} = -274 \times 10^{-12}$ C/N, was replaced with an effective piezoelectric coefficient, d_{31}^{eff}, because of the stress biasing using

$$d_{31}^{\text{eff}} = k_p d_{31} = 2.7 d_{31}. \tag{14}$$

In addition to the modified piezoelectric coefficient, the coefficient of thermal expansion was also necessary for both the PZT and the reduced layer. The material properties used for the actuator analysis are also given in the appendix.

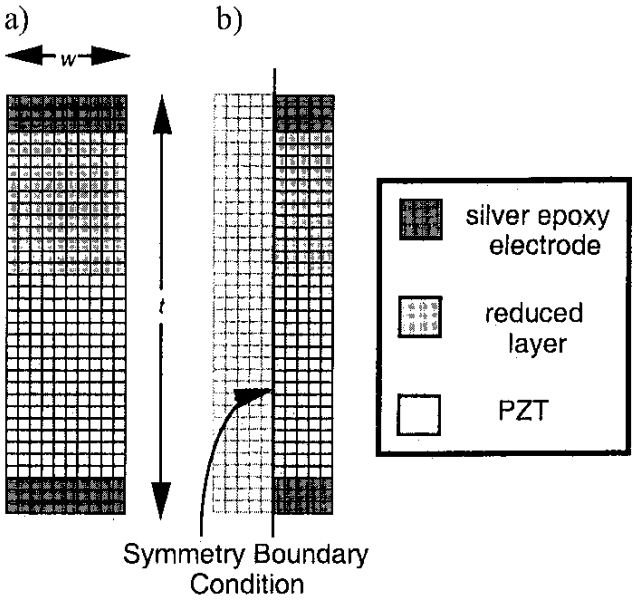

Fig. 4. 2-D model of a free, single, linear array element of RAINBOW material: (a) mesh of the full element and (b) reduced mesh using the symmetry boundary condition.

III. FEA Results

A. Ultrasound Characterization

To verify the assumption that the RAINBOW material can be modeled by a reduced layer and an active piezoelectric layer and to check the material properties of the reduced layer, we first simulated the vector impedance of a single, free, linear array element of RAINBOW material in air. Because of the long length of the element ($l/t \approx 30$), a 2-D model, with the electric charge scaled by the length of the element, was used for calculation as shown in Fig. 4(a). The silver epoxy electrodes were also included in the model because they were approximately $\lambda/10$ thick at 4.2 MHz. The size of the model was reduced further by modeling one-half the width of the element with a symmetric boundary condition as shown in Fig. 4(b). To minimize numerical

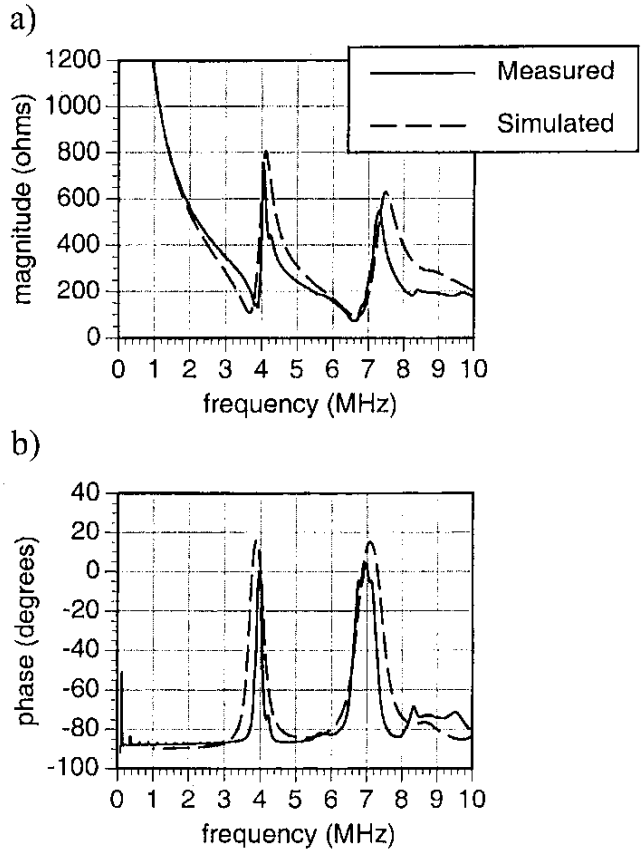

Fig. 5. Comparison of measured and simulated electrical impedance of a free linear array element of RAINBOW material: (a) magnitude and (b) phase.

dispersion, the model was discretized with at least 10 elements per wavelength at the highest frequency of interest (10 MHz) [21], and calculation of vector impedance was completed in roughly 10 min. Fig. 5(a) compares the simulated and measured magnitudes, and Fig. 5(b) compares the simulated and measured phases. The FEA accurately predicted the two resonances of the vector impedance of the free linear array element at approximately 4.2 and 7.5 MHz. To determine the source of the two resonances, the resonance shapes were calculated at both frequencies. Fig. 6(a) and (b) show the minimum and maximum displacement of the resonance shape at 4.2 MHz, respectively. This mode corresponds to the thickness mode of the entire RAINBOW stack. Fig. 6(c) and (d) correspond to the resonance shape at 7.5 MHz. This mode exhibits more lateral motion and corresponds to the thickness resonance of the piezoelectric layer coupled with the reduced layer and electrodes.

With the encouraging FEA of the free single element, we increased the complexity of the model to calculate the vector impedance of a deformable array element in air. Similar to the previous calculation, we used a 2-D model of one-half the width of the element with a symmetry boundary condition as shown in Fig. 7. To reduce the complexity, even though only a portion of the deformable array element was bonded to the pedestal, the pedestal sufficiently damped the element such that we modeled epoxy behind the whole element. In addition to the epoxy pedestal, the matching layer was also modeled. Calculation of vector impedance of the deformable array element was completed in roughly 15 min. Fig. 8(a) compares the simulated and measured magnitudes, and Fig. 8(b) compares the simulated and measured phases. The resonance visible at 2.9 MHz is due to the thickness resonance of the matching layer coupled with the element. The two resonances at 4.5 and 5.5 MHz are both thickness modes of the RAINBOW ceramic coupled with more lateral modes in the matching layer and electrodes. The multiple resonances around 7.5 MHz are due to the thickness resonance of the PZT layer coupled with lateral modes in the backing and electrodes. The simulated vector impedance is in good agreement with measurement.

Next, we simulated the pulse-echo sensitivity of a single deformable array element in water. For the measurement, the element was driven with a 4.2-MHz, 100-Vpp, two-cycle sine wave with a polished aluminum block 5 cm from the transducer face. The simulation was completed under the same driving conditions with an infinite, perfect reflector 5.0 cm from the transducer. In addition, both the transmitter and receiver impedances were included in the model. Because reflections caused by water behind the element and the damping effect of the pedestal were also considered important to calculate the pulse shape, we used a 3-D model for this calculation as shown in Fig. 9. To complete both the send and receive problems with the 3-D model, roughly 5 h were necessary. The comparison of the simulated and measured pulse-echo sensitivities and the corresponding power spectrums is shown in Fig. 10(a) and (b), respectively. The FEA is in good agreement with measurement. To achieve a closer match between measurement and the FEA, the composition of the deformable array element should be further investigated. For example, irregularities in the bond lines between the deformable array and pedestal could contribute to the discrepancy at the tail of the pulse. Another possible area of improvement includes the uniformity of the silver electrodes on the actuator, which varied by 0.015 mm over the length of the actuator.

B. Low Frequency Actuator Characterization

To verify the bending mode of the actuator, the low frequency vector impedance in air was simulated using PZFlex. Because experimental comparisons of low frequency displacement with and without the ultrasound matching layer were extremely similar, the required simulation time was decreased by omitting the matching layer from the model. The silver epoxy electrodes were also omitted to decrease simulation time. In addition, the portion of the actuator bonded to the pedestal was modeled by fixing the corresponding nodes in place. The 2-D model used for the calculation is shown in Fig. 11, and vector impedance calculations were computed in approximately

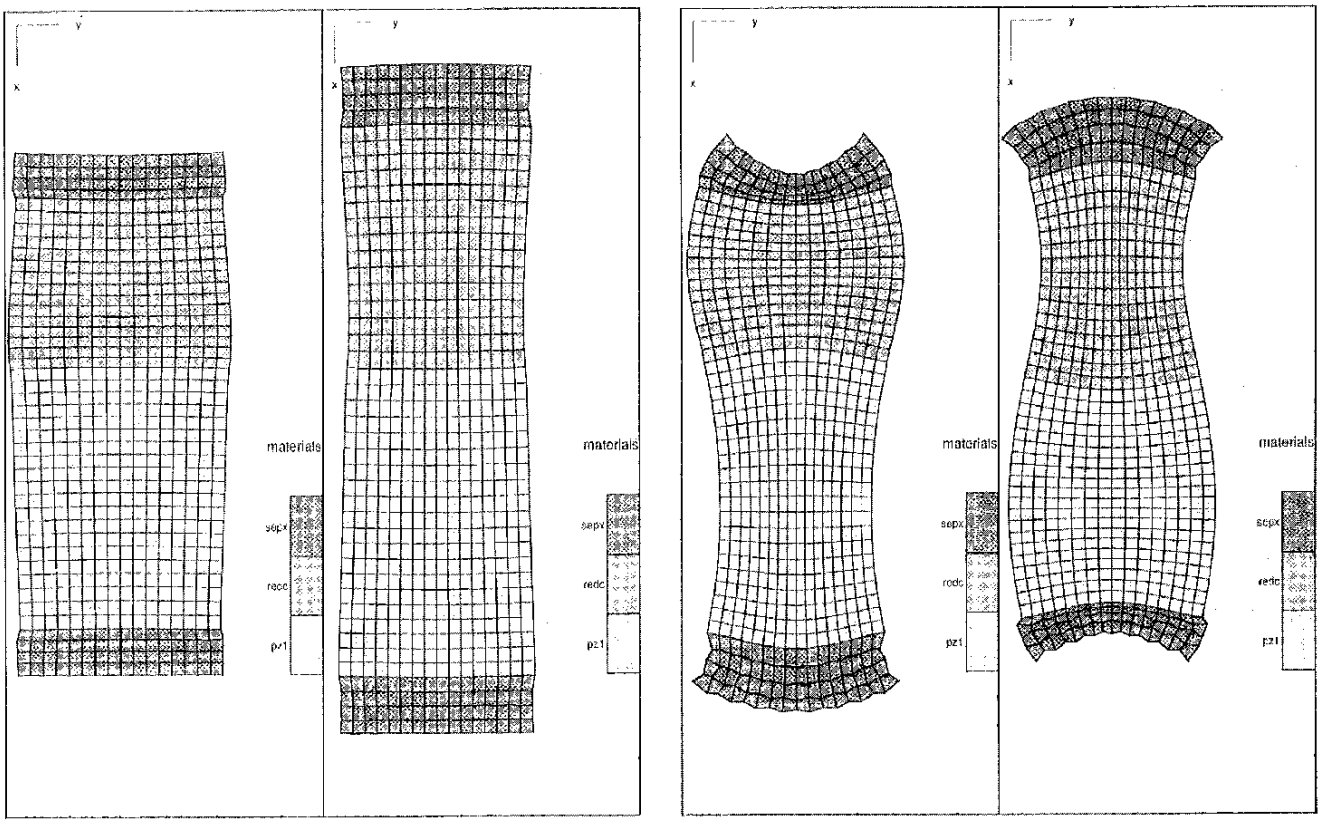

Fig. 6. Resonance shapes of the free, linear array element of RAINBOW material: (a) minimum displacement at 4.2 MHz, (b) maximum displacement at 4.2 MHz, (c) minimum displacement at 7.5 MHz, and (d) maximum displacement at 7.5 MHz.

30 min. The comparison of the simulated versus measured low frequency vector impedance is shown in Fig. 12. The fundamental flexure resonance of the actuator is correctly predicted at 1.3 kHz, followed by the first overtone at 8.8 kHz, and the second overtone at 24.3 kHz. The frequencies of the first and second overtones are slightly overestimated by the simulation compared with the measurement. Using (4), the theoretical flexure resonance is calculated to be 1.5 kHz using only the free length of the actuator, 10.7 mm. The first and second overtone frequencies are then predicted to be 9.45 and 27.0 kHz, respectively. Because both the simulation of the low frequency impedance and theory slightly over estimate the flexure frequencies, this discrepancy is possibly due to the bond of the element to the pedestal. The bond producing the cantilever configuration may be more compliant than the fixed nodes in the simulation or the perfect constraints assumed in theory. Also, a more extensive investigation of damping in the RAINBOW could potentially lead to a better match between simulation and experiment.

Using ANSYS, we next modeled the initial curvature and voltage-induced bending of the actuator. The 3-D model used for the ANSYS simulations is shown in Fig. 13, again omitting the matching layer and electrodes. To calculate the initial curvature, the thermal stresses developed from cooling from 975 to 20°C were modeled, and the deflection of the tip of the actuator from the horizontal position was recorded. The simulated deflection of the actuator tip caused by the curvature was 0.87 mm compared with the measured offset of 0.80 mm.

Once the initial curvature was calculated, the voltage-induced bending was modeled. A magnified picture of the actual displacement of a deformable array element in response to an applied voltage of 500 V DC is shown of Fig. 14(a). The first actuator of the array has been tilted down, toward the pedestal. The remaining actuators have not been tilted so that the tip displacement can be visualized. Fig. 14(b) is the simulated comparison of tip displacement calculated using ANSYS with an applied voltage of 500 V DC. The dashed outline represents the control element without voltage, and the solid outline represents the tilted actuator. To compare the tip displacement with measurement for a range of applied voltages, the free deflection of the actuator was recorded as a function of increasing voltage. Accordingly, nonlinear effects such as hysteresis were not included in the simulation. Fig. 15 compares the measured and simulated tip displacement of the actuator from 0 to 500 V. The measured and simulated tip displacements are in good agreement.

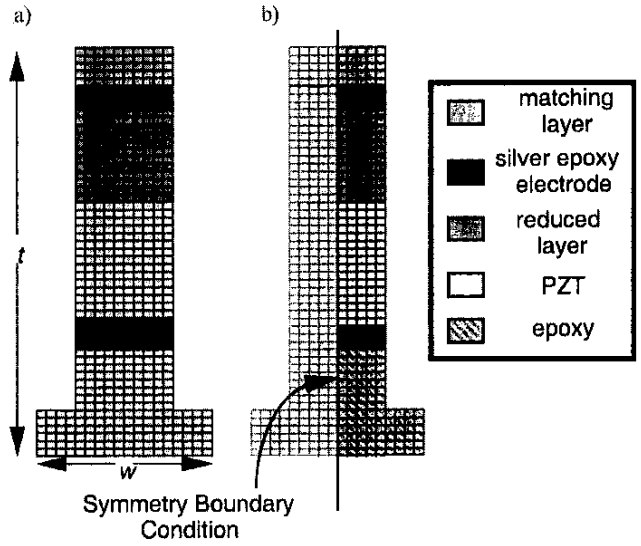

Fig. 7. 2-D model of a single deformable array element: (a) mesh of the full element and (b) reduced mesh using the symmetry boundary condition.

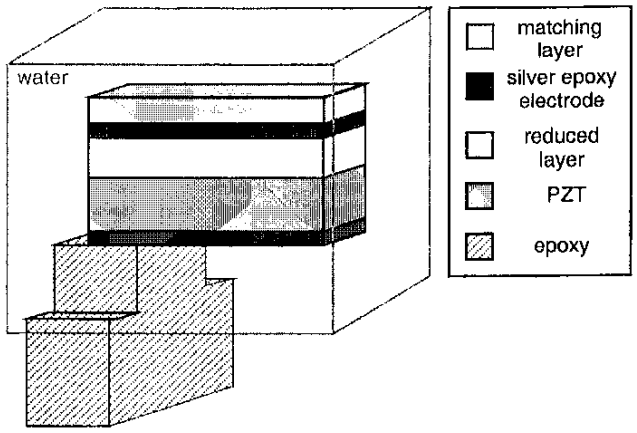

Fig. 9. 3-D model of a single deformable array element for pulse-echo simulations.

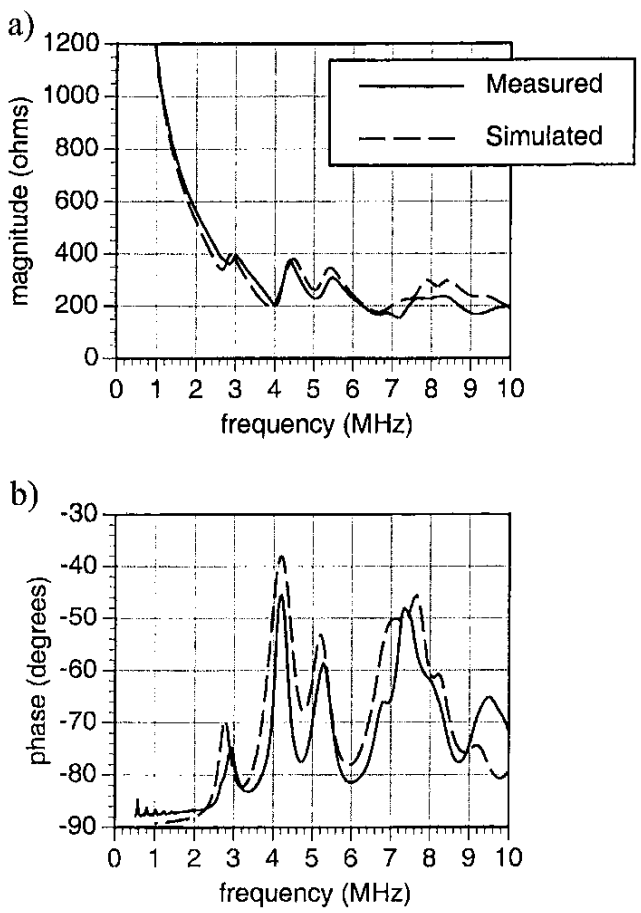

Fig. 8. Comparison of measured and simulated electrical impedance of a deformable array element: (a) magnitude and (b) phase.

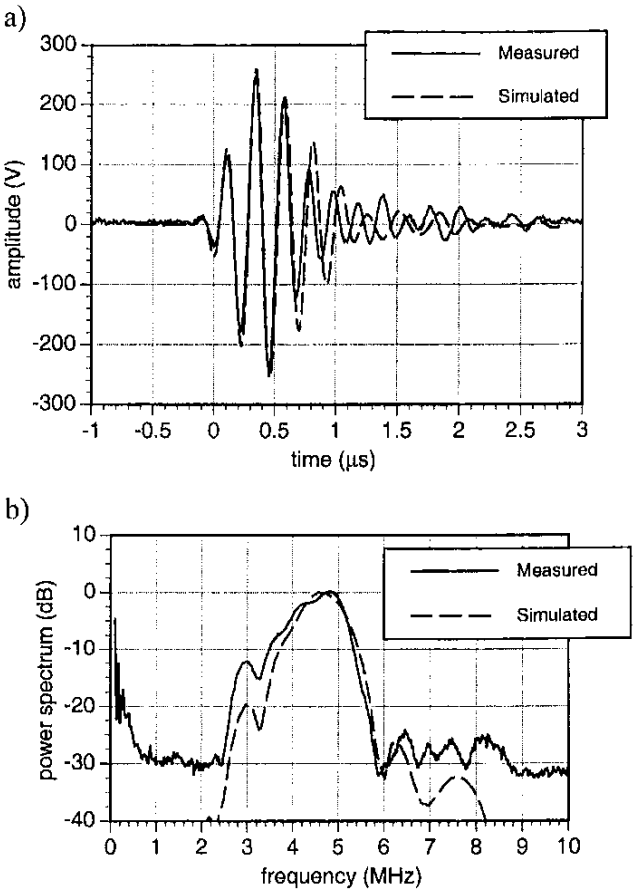

Fig. 10. Comparison of measured and simulated pulse-echo sensitivity and corresponding power spectrum: (a) pulse-echo sensitivity and (b) power spectrum.

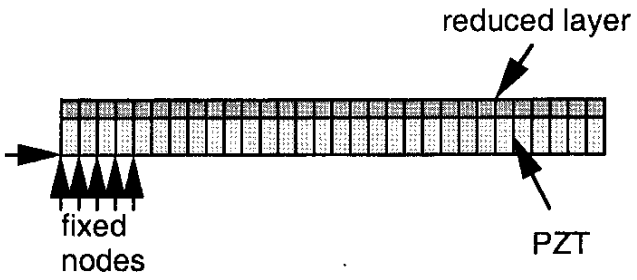

Fig. 11. 2-D model of a RAINBOW element in a cantilever configuration for the low frequency impedance simulation.

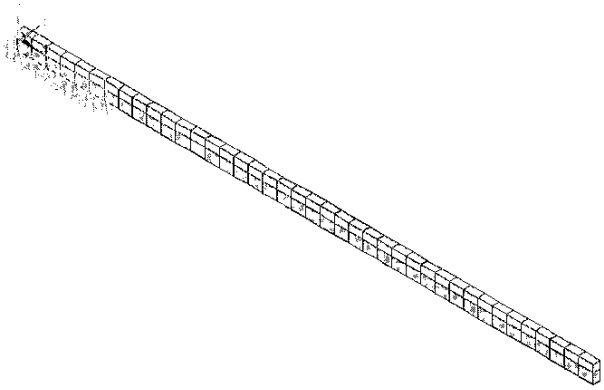

Fig. 13. 3-D model of RAINBOW element cantilever configuration for the initial curvature and voltage-induced bending simulations.

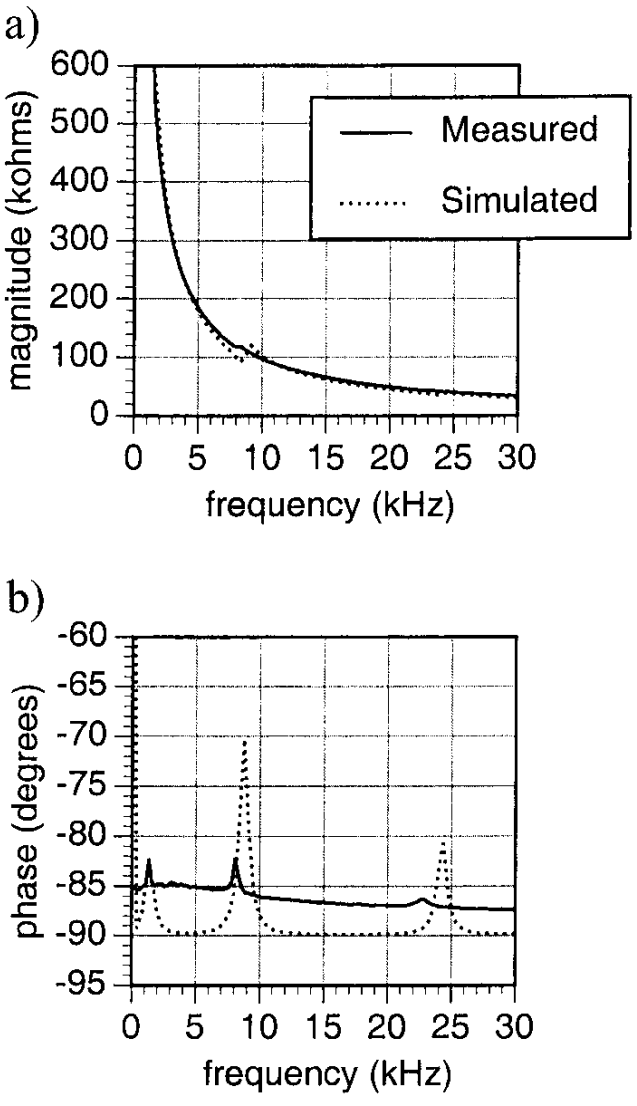

Fig. 12. Comparison of the measured and simulated low frequency impedance of a RAINBOW element: (a) magnitude and (b) phase.

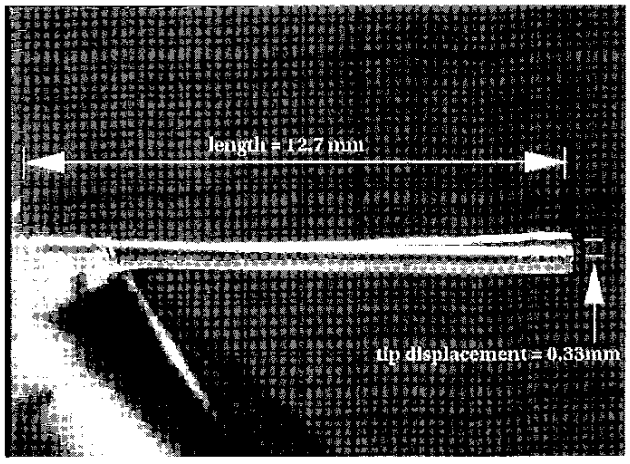

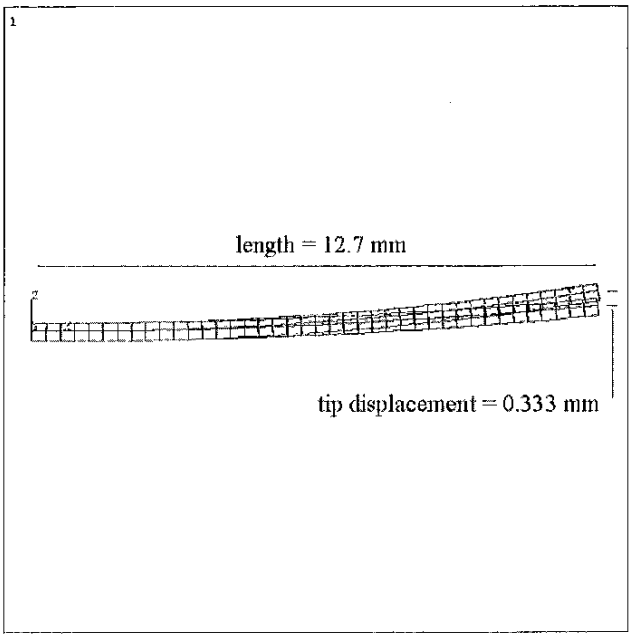

Fig. 14. Magnified picture of RAINBOW actuator displacement: (a) displacement of an element of the deformable array and (b) simulated displacement.

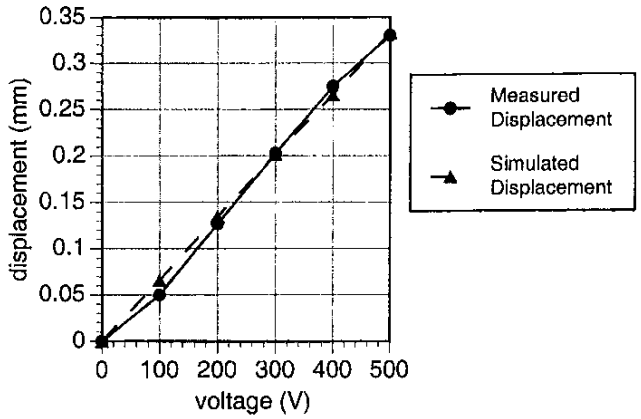

Fig. 15. Comparison of measured and simulated tip displacements for applied voltages ranging from 0 to 500 V DC.

IV. Conclusion

We have successfully modeled both ultrasound characteristics and low frequency actuator characteristics of the deformable array using both 2-D and 3-D FEA. The ultrasound characterization included simulations of vector impedance of a free, single RAINBOW element along with the more complicated deformable array element with a backing and matching layer. For both elements, the simulation accurately predicted measured vector impedance. In addition, simulations of pulse-echo sensitivity and corresponding bandwidth of single deformable array elements were also performed and were a good match to measurement.

The low frequency actuator characterization included simulations of vector impedance, initial curvature, and voltage-induced deflection. The low frequency vector impedance simulation accurately predicted the frequency of the fundamental flexure resonance of the cantilever configuration and slightly overestimated the first and second overtone frequencies. The 1.3-kHz fundamental flexure resonance offers strong potential for real-time interactive phase correction as well as adjustable elevation focusing.

The simulation of the initial curvature caused by the cooling process of RAINBOW fabrication predicted an offset of 0.87 mm compared with the measured offset of 0.80 mm. Finally, simulations of voltage-induced deflection accurately predicted the measured deflection for applied voltages ranging from 0 to 500 V DC.

We have successfully employed FEA to predict both low frequency actuator characteristics and ultrasound characteristics of the complex deformable array structure. This work is the first step toward using 2-D and 3-D FEA as a design tool for deformable array development. Based on these promising results, we believe that FEA may be used to improve further the performance of future deformable transducer designs while minimizing fabrication effort.

Acknowledgments

We acknowledge Weidlinger Associates, Inc. for the many technical consultations throughout the course of this work. The guidance of Najib Abboud, Dave Vaughan, and David Powell was invaluable, and their accessibility most appreciated. We would thank Gene Haertling for helpful conversation and Aura Ceramics, Inc. for providing the RAINBOWs used in this investigation.

Appendix

c^E is the elastic constant in the presence of a constant electric field.

e is the piezoelectric stress constant.

$\varepsilon/\varepsilon_0$ is the relative dielectric constant.

ρ is the density.

Q is the mechanical damping.

d is the piezoelectric constant stress constant.

A. Material Data for Ultrasound Characterization

1. PZT 5H:

$$c^E = \begin{bmatrix} 12.60 & 7.95 & 8.41 & 0.0 & 0.0 & 0.0 \\ & 12.60 & 8.41 & 0.0 & 0.0 & 0.0 \\ & & 11.70 & 0.0 & 0.0 & 0.0 \\ & & & 2.30 & 0.0 & 0.0 \\ & & & & 2.30 & 0.0 \\ & & & & & 2.32 \end{bmatrix} \times 10^{10}\text{N/m}^2$$

$$\rho = 7500\text{kg/m}^3,\ Q = 35$$

$$e = \begin{bmatrix} 0.0 & 0.0 & 0.0 & 0.0 & 17.0 & 0.0 \\ 0.0 & 0.0 & 0.0 & 17.0 & 0.0 & 0.0 \\ -6.5 & -6.5 & 23.3 & 0.0 & 0.0 & 0.0 \end{bmatrix} \text{C/m}^3$$

$$\varepsilon^T/\varepsilon_0 = \begin{bmatrix} 1700 & 0 & 0 \\ 0 & 1700 & 0 \\ 0 & 0 & 1470 \end{bmatrix}$$

2. Reduced Layer:

$$c = \begin{bmatrix} 8.0 & 3.5 & 3.5 & 0.0 & 0.0 & 0.0 \\ & 8.0 & 3.5 & 0.0 & 0.0 & 0.0 \\ & & 8.0 & 0.0 & 0.0 & 0.0 \\ & & & 2.56 & 0.0 & 0.0 \\ & & & & 2.56 & 0.0 \\ & & & & & 2.56 \end{bmatrix} \times 10^{10}\text{N/m}^2$$

$$\rho = 7500\text{kg/m}^3,\ \varepsilon/\varepsilon_0 = 2940,\ Q = 9$$

3. Ablefilm Matching Layer:

$$\rho = 3600\text{kg/m}^2 \quad \text{bulk velocity} = 1650\text{m/s}$$
$$\text{shear velocity} = 800\text{m/s} \quad \text{damping } Q = 8$$

4. Silver Epoxy:

$$\rho = 2710\text{kg/m}^2 \quad \text{bulk velocity} = 1900\text{m/s}$$
$$\text{shear velocity} = 980\text{m/s} \quad \text{damping } Q = 20$$

5. Epoxy:

$$\rho = 1160\text{kg/m}^2 \quad \text{bulk velocity} = 2620\text{m/s}$$
$$\text{shear velocity} = 1150\text{m/s} \quad \text{damping } Q = 15$$

B. Material Data for the Low Frequency Actuator Characterization

1. PZT 5H

$$d = \begin{bmatrix} 0 & 0 & 0 & 0\,0\,0 \\ 0 & 0 & 0 & 0\,0\,0 \\ 7.38 & 2.74 & 5.94 & 0\,0\,0 \end{bmatrix} \times 10^{10}\text{C/N}$$

$$\alpha_{\text{PZT}} = 0.44 \times 10^{-5}\,^{\circ}\text{C}^{-1}, \ \alpha_{\text{rodc}} = 0.88 \times 10^{-5}\,^{\circ}\text{C}^{-1}.$$

REFERENCES

[1] L. L. Ries and S. W. Smith, "Phase aberration correction in two dimensions using a deformable array transducer," *Ultrason. Imag.*, vol. 17, pp. 227–247, 1995.

[2] ——, "Phase aberration correction in two dimensions using an integrated deformable actuator/transducer," *IEEE Trans. Ultrason., Ferroelect., Freq. Contr.*, vol. 44, no. 6, pp. 1366–1375, 1997.

[3] J. W. Hardy, "Adaptive optics," *Sci. Amer.*, pp. 60–65, Jun, 1994.

[4] L. L. Ries, S. W. Smith, and G. E. Trahey, "Two-dimensional phase correction using a deformable ultrasonic transducer array," US Patent # 5605154, 1997.

[5] G. H. Haertling, "Rainbow ceramics – A new type of ultra-high-displacement actuator," *Amer. Ceram. Soc. Bull.*, vol. 73, no. 1, pp. 93–96, 1994.

[6] C. Ellissalde, L. E. Cross, and C. A. Randall, "Structural-property relations in a reduced and internally biased oxide wafer (RAINBOW) actuator material," *J. Amer. Ceram. Soc.*, vol. 79, no. 8, pp. 2041–2048, 1996.

[7] G. Li and G. H. Haertling, "The piezoelectric, pyroelectric, and photoelectronic properties of PLZT RAINBOW ceramics," in *Proc. IEEE ISAF*, East Brunswick, NJ, 1996, pp. 907–910.

[8] S. Chandran, V. D. Kugel, and L. E. Cross, "Characterization of the linear and non-linear dynamic performance of RAINBOW actuator," in *Proc. IEEE ISAF*, East Brunswick, NJ, 1996, pp. 743–746.

[9] J. K. Lee and M. A. Marcus, "The deflection-bandwidth product of poly(vinylidene fluoride) benders and related structures," *Ferroelectrics*, vol. 32, pp. 93–101, 1981.

[10] J. G. Smits and W. Choi, "The constituent equations of piezoelectric heterogeneous bimorphs," *IEEE Trans. Ultrason., Ferroelect., Freq. Contr.*, vol. 38, no. 3, pp. 256–270, 1991.

[11] J. G. Smits, S. I. Dalke, and T. K. Cooney, "The constituent equations of piezoelectric bimorphs," *Sens. Actuators A*, vol. 28, no. 1, pp. 41–61, 1991.

[12] V. D. Kugel, S. Chandran, and L. E. Cross, "Caterpillar-type piezoelectric d33 bimorph transducer," *Appl. Phys. Lett.*, vol. 69, no. 14, pp. 2021–2023, 1996.

[13] G. H. Haertling, "Stress-induced effects in PLZT ceramics," in *Proc. 10th IEEE ISAF*, 1996, pp. 65-68.

[14] G. Li, E. Furman, and G. H. Haertling, "Stress-enhanced displacements in PLZT rainbow actuators," *J. Amer. Ceram. Soc.*, vol. 80, no. 6, pp. 1382–1388, 1997.

[15] V. D. Kugel, S. Chandran, and L. E. Cross, "A comparative analysis of piezoelectric bending-mode actuator," in *SPIE's 4th Ann. Symp. Smart Structures Materials*, San Diego, CA, 1997, pp. 70–80.

[16] J. van Randeraat and R. E. Setterington. *Piezoelectric Ceramics*. London: Mullard Limited, 1974.

[17] J. A. Hossack and G. Hayward, "Finite-element analysis of 1-3 composite transducers," *IEEE Trans. Ultrason., Ferroelect., Freq. Contr.*, vol. 38, no. 6, pp. 618–629, 1991.

[18] R. Lerch, "Simulation of piezoelectric devices by two- and three-dimensional finite elements," *IEEE Trans. Ultrason., Ferroelect., Freq. Contr.*, vol. 37, no. 3, pp. 233–247, 1990.

[19] M. R. Draheim and W. Cao, "Finite element analysis on impedance matching layer thickness," in *Proc. IEEE ISAF*, East Brunswick, NJ, 1996, pp. 1015–1017.

[20] R. L. Goldberg, M. J. Jurgens, D. M. Mills, C. S. Henriquez, D. Vaughan, and S. W. Smith, "Modeling of piezoelectric multilayer ceramics using finite element analysis," *IEEE Trans. Ultrason., Ferroelect., Freq. Contr.*, vol. 44, no. 6, pp. 1204–1214, 1997.

[21] G. L. Wojcik, D. K. Vaughan, N. Abboud, and J. Mould, "Electromechanical modeling using explicit time-domain finite elements," in *Proc. IEEE Ultrason. Symp.*, Baltimore, MD, 1993, pp. 1107–1112.

[22] Y. Kagawa and G. M. Gladwell, "Finite element analysis of flexure-type vibrators with electrostrictive transducers," *IEEE Trans. Sonics Ultrason.*, vol. SU-17, no. 1, pp. 41–49, 1970.

[23] D. T. Detwiler, M. Shen, and V. B. Venkayya, "Finite element analysis of laminated composite structures containing distributed piezoelectric actuators and sensors," *Finite Elements Anal. Design*, vol. 20, no. 2, pp. 87–100, 1995.

[24] E. Furman, G. Li, and G. H. Haertling, "Electromechanical properties of rainbow devices," in *Proc. IEEE ISAF*, University Park, PA, 1994, pp. 146–149.

[25] G. Wojcik, C. DeSilets, L. Nikodym, D. Vaughan, N. Abboud, and J. Mould, "Computer modeling of diced matching layers," in *Proc. IEEE Ultrason. Symp.*, San Antonio, TX, 1996, pp. 1503–1508.

[26] N. N. Abboud, G. L. Wojcik, D. K. Vaughan, J. Mould, D. J. Powell, and L. Nikodym, "Finite element modeling for ultrasonic transducers," in *Proc. SPIE Int. Symp. Med. Imag.*, San Diego, CA, 1998, pp. 19–42.

[27] R. Lerch, H. Landes, and H. T. Kaarmann, "Finite element modeling of the pulse-echo behavior of ultrasound transducers," in *IEEE Ultrason. Symp.*, Cannes, France, pp. 1021–1025, 1994.

Loriann L. Ries received the B. S. degree in Biomedical Engineering from Case Western Reserve University, Cleveland, OH, in 1991 and the Ph.D. degree in Biomedical Engineering from Duke University, Durham, NC, in 1998. Her graduate research included medical ultrasound transducer design and fabrication with applications for phase abberation correction. Upon finishing her graduate degree, she joined ATL Ultrasound, where she continues to work in medical ultrasound transducers as an Acoustic Design Engineer.

Stephen W. Smith (M'91) was born in Covington, KY, on July 27, 1947. He received the B.S. degree in physics in 1967 from Thomas More College, Ft. Mitchell, KY, the M.S. degree in physics in 1969 from Iowa State University, Ames, and the Ph.D degree in biomedical engineering in 1975 from Duke University, Durham, NC.

In 1969, he became a Commissioned Officer in the U.S. Public Health Service, assigned to the Food and Drug Administration, Center for Devices and Radiological Health, Rockville, MD, where he worked until 1990 in the study of medical imaging, particularly diagnostic ultrasound and the devel-

opment of performance standards for such equipment. In 1978, he became Adjunct Associate Professor of Radiology at Duke University Medical Center. In 1990, he became Associate Professor of Biomedical Engineering and Radiology and Director of Undergraduate Studies in Biomedical Engineering at Duke University. He holds 14 patents in medical ultrasound and has authored 120 papers in the field.

Dr. Smith has served on the education committee of the American Institute of Ultrasound in Medicine, the Executive Board of the American Registry of Diagnostic Medical Sonographers, and the Editorial Board of *Ultrasonic Imaging*. He was co-recipient of the American Institute of Ultrasound in Medicine Matzuk Award in 1988 and 1990 and the IEEE UFFC best paper award in 1984 and 1995. He is also a founder of Volumetrics Medical Imaging, Inc.